Influence of clay organic modifier on the thermal-stability of PLA based nanocomposites

A. Araújo [a,b], G. Botelho [a,*], M. Oliveira [b], A.V. Machado [b]

[a] Chemistry Center/Department, University of Minho, Campus de Gualtar, 4710-057 Braga, Portugal

[b] IPC - Institute for Polymers and Composites, I3N, University of Minho, Campus de Azurém, 4800-058 Guimarães, Portugal

Keywords:

Thermo-oxidative degradation
PLA
Nanocomposites
Clay minerals

Abstract

Poly(lactic acid) (PLA) is a biodegradable aliphatic thermoplastic polyester well known for being a promising alternative to petroleum-based materials since it can be produced from renewable resources. Although this polymer has good properties when compared to other biodegradable polymers, it presents some limitations like poor thermal, mechanical resistance and gas barrier. The incorporation of clay minerals has been used as a way to overcome this problem. The present work aims to investigate the influence of clay organic modifier (Cloisite 30B, Cloisite 15A and Dellite 43B) and amount (3 and 5%) on PLA thermal stability. PLA and PLA nanocomposites were submitted to thermo-oxidative degradation at 140°C during 120 h . Samples removed along the time were characterized by gel permeation chromatography (GPC), scanning electron microscopy (SEM), X-ray diffraction (XRD), nuclear magnetic resonance (^{1}H NMR), Fourier transform infrared spectroscopy (FTIR) and differential scanning calorimetry (DSC). After degradation, even though all samples exhibited a significant decrease of molecular weight, it was smaller for nanocomposites. As a consequence of chain scission an increase in the crystallinity degree was observed for all nanocomposites. Results showed that clay mineral incorporation, mainly D43B enhanced the polymer thermal stability.

Introduction

The packaging industry is an important economic sector, which deals with high quantities of plastic materials. Packages made from petroleum-based polymers are usually discarded after the first use, and their elimination and reintegration into the carbon cycle can require hundreds or even thousands of years (Badía et al., 2011). Due to the negative impact of plastic waste on the environment, biodegradable polymers have recently attracted great interest to the scientific community. Among the biodegradable polymers, PLA is the one that can be used as a promising alternative to the petroleumbased commodity polymers (Badía et al., 2011; Fukushima et al., 2009; Rhim et al., 2009; Zaidi et al., 2010), because it can be produced from renewable resources, such as, corn, potato, sugar beet and other agricultural products (Gardette et al., 2011; Zaidi et al., 2010). Moreover, its production consumes carbon dioxide (Picard et al., 2011) and its degradation does not exhibit any eco-toxicological effect (Bordes et al., 2009). Nonetheless, due to economical speculation, the productions of biopolymers from agriculture sources are facing a paradox. Farmers are tempted to abandon cheap food production in favor of producing higher value-in-use crops offering much higher profits. In 2007, Mexico faced the "Mexican Tortilla Crisis" provoked by financial speculation on maize, which triggered a dramatic rise in

its cost, threatening the health and sustenance of the poor countries (Mülhaupt, 2013).

PLA is a linear aliphatic thermoplastic polyester (Chang et al., 2003a; Sinharay and Bousmina, 2005) that can be synthesized from lactic acid monomer or by ring-opening polimerization of lactide monomers (Bikiaris, 2011). It has several interesting properties, including thermoplasticity, high degree of transparency, biocompatibility and processability using conventional processing equipment (Badía et al., 2011; Zaidi et al., 2010; Zhou and Xanthos, 2009). Additionally lactide can be recovered by thermal degradation (Nishida et al., 2003). The main limitations of this biodegradable polymer are poor thermal, mechanical resistance and gas barrier properties (Bikiaris, 2011), which are essential characteristics to the packaging industry. However, published results have shown that these properties can be enhanced by the addition of low amounts of clay minerals, mainly organic modified montmorillonite (Mt) (Lewitus et al., 2006; Wu and Wu, 2006; Wu et al., 2009; Zhu et al., 2011).

Since these are new materials, it is relevant to investigate the stability of PLA nanocomposites under different conditions (e.g., hydrolytic, enzymatic, microbial, UV radiation, photo-oxidative, thermal, natural weathering) (Carrasco et al., 2011; Chow and Lok, 2009; Fukushima et al., 2009; Gardette et al., 2011; Nieddu et al., 2009; Paul et al., 2005).

According to published data, PLA degradation depends on several parameters, such as, molecular weight, crystallinity, purity, temperature, pH , presence of terminal carboxyl or hydroxyl groups, water permeability, and additives acting catalytically that may include enzymes,
bacteria or inorganic fillers (Carrasco et al., 2010; Zhou and Xanthos, 2009). Moreover, thermal degradation of PLA occurs by several mechanisms, such as, (a) hydrolysis by trace amounts of water, (b) zipperlike depolymerization, (c) oxidative, random main-chain scission, (d) intermolecular transesterification to monomer and oligomeric esters, and (e) intramolecular transesterification resulting in monomer and oligomer lactides of low molecular weight formation (Madhavan Nampoothiri et al., 2010).

Most of the research studies that have been performed on thermal stability of PLA use thermogravimetry (TGA), both under air and nitrogen (Zhou and Xanthos, 2009). Some authors showed that clays significantly increased the PLA thermal stability under thermo-oxidative conditions (Pluta et al., 2002; Zhou and Xanthos, 2009). Also, an increase in thermal stability with increasing nanoclay content up to 5wt.% in PLLA plasticized with polyethylene glycol was observed. However, other authors (Chang et al., 2003b) reached opposite conclusions, the thermal stability under nitrogen decreased linearly as the amount of clay increased from 2 to 8wt%. Liu et al. studied the thermo-oxidative degradation of PDLLA both under air and nitrogen without the presence of nanoclays and find out that the degradation proceed by a random chain scission mechanism with two or three stages. The first stage was dominated by the oligomers containing carboxylic acid groups and hydroxyl groups, during which oxygen and nitrogen had little effect on degradation. When the oligomers were consumed over or evaporated, the 2nd stage begins, and oxygen has a promoting effect on the thermo-oxidation. The third stage of PDLLA was observed when it was degraded under nitrogen over 200°C, which was caused by the appearance of carboxylic acids. The authors also suggest the importance of removing low molecular oligomers, especially those containing hydroxyl and carboxylic acid groups, and the importance of polymer protection from air when they are in the molten state (Liu et al., 2006).

Therefore, the present work aims to investigate the effect of different organically modified Mts (Cloisite 30B, Cloisite 15A and Dellite 43B) and their amounts on PLA thermo-oxidative aging. Samples were prepared by melt mixing, placed in an oven, collected along the time and characterized by several analytical techniques.

Experimental

Materials

The commercial PLA grade (3251D) was supplied by NatureWorks LLC (USA). The three modified Mts used were supplied by Southern Clay Products (USA) (Cloisite 30B and Cloisite 15A) and Laviosa Mineraria (Italy) (Dellite 43B). The main characteristics of the clay minerals are presented in Table 1. Chloroform and deuterated chloroform were purchased from Lab-Scan and Acros Organics, respectively, and used as received.

Sample preparation

Polymer pellets and modified Mt were dried in a vacuum oven at 60 °C for 12 h before use. PLA nanocomposites with 3 and 5wt.% of C15A, C30B and D43B were prepared in a Haake batch mixer (HAAKE Rheomix 600 OS; volume 69 cm^3) equipped with two rotors running in a counter-rotating way. Polymer and each clay were pre-mixed and added together to the batch mixer chamber, the rotor speed was 80 rpm , the set temperature was 190 °C. After mixing during 5 min the total sample was removed.

The prepared nanocomposites were then pressed into thin films at 200 °C under 30 tons for 60 s . The thickness of each film (ca. 40μm) was measured with a pachymeter Mitutoyo.

Thermal degradation

Thin films of PLA and PLA nanocomposites were cut into small rectangular sections (100 × 25 mm). Thermo-oxidative degradation experiments were carried out in an oven under air at 140°C along 120 h .

Characterization

Scanning electron microscopy (SEM)

The samples were fractured in liquid nitrogen and after gold plating the morphology was analyzed using a Leica Cambridge S360 scanning electron microscope.

X-ray diffraction (XRD)

The diffraction patterns were obtained using a diffractometer (AXS Nanostar-D8 Discover, Bruker) equipped with a CuK α generator ($\lambda = 1.5404$Å) at 40 kV and 40 mA , in a 2θ range from 0.08 to 10°. The clay minerals were analyzed directly, whereas the nanocomposite samples were previously compression molded into disks with a diameter of 20 mm and a thickness of 4 mm .

3. ^{1} H nuclear magnetic resonance spectroscopy (^{1} H NMR)

^{1} H NMR spectra of initial and degraded PLA samples were recorded on a Varian Unity Plus 300 MHz spectrometer using deuterated chloroform as solvent and tetramethylsilane as internal standard.

Gel permeation chromatography (GPC)

The number (Mn) and weight average (Mw) molar mass and polydispersity (Ip) were measured by GPC. Solutions were prepared in

Table 1
Clay properties.

Commercial name	Modifier structure [a]	Extent of modification (meq/100 g clay)	Particle size (μm)	% moisture	Specific gravity (g/cm^3)	Code
Cloisite 30B	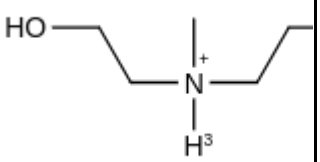	90	≤ 2 (10%) ≤ 6 (50%) ≤ 13 (90%)	<2	1.98	C30B

Cloisite 15A	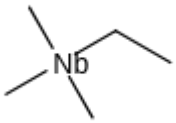	125	≤ 2 (10%) ≤ 6 (50%) ≤ 13 (90%)	<2	1.66	C15 A
Dellite 43B	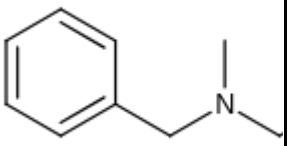	66	7-9	3 (max)	1.4	D4 3B

tetrahydrofuran (99.9%) and prefiltered on filter disk (hydrophobic polytetrafluoroethylene, 0.45μ m pore size) before injection. The analysis was performed in a SEC Waters 150-CV apparatus equipped with 3 Waters Ultrastyragel columns (HR1 and HR4; inner diameter = 7.8 mm , length = 300 mm and particle size = 5μ m) and with viscometer and refractometer detectors. Chloroform was used as eluent with a flow rate of 1 mL/min at 23°C. The calibration curve was previously obtained with polymethylmethacrylate standards with narrow molar mass distribution.

Fourier transform infrared spectroscopy (FTIR)

Room temperature infrared spectra of the initial and degraded films were recorded on an ABB FTLA 2000 spectrometer in the range $4000 - 500\ cm^{-1}$ by averaging 16 scans and using a resolution of $4\ cm^{-1}$.

Differential scanning calorimetry (DSC)

Thermal properties were determined in a Perkin-Elmer DSC 7 under nitrogen. Approximately 6 mg of each sample was cut from the films and placed in an aluminum pan. The analysis was performed in three steps: first heating from 30 to 250°C at 50°C/min, cooling from 250 to 30°C at 10°C/min, and second heating from 30 to 250°C at 10°C/min. Two minute isothermal plateau was inserted between the ramps. The glass transition temperature (T_g), cold crystallization temperature (T_{cc}), melting temperature (T_m), cold crystallization enthalpy (ΔH_{cc}), and melting enthalpy (ΔH_m) were determined from second heating curves. Crystallization and melting temperatures were taken at the maximum of the crystallization exotherm (T_{cc}) or of the melting endotherm (T_m). The crystallinity degree (χ_c) was obtained using Eq. (1):

$$\chi_c(\%) = \left(\frac{\Delta H_m - \Delta H_{cc}}{\Delta H_m^0 \times \left(1 - \frac{\text{wt. \% clay}}{100}\right)} \right) \times 100 \qquad (1)$$

where ΔH_m and ΔH_{cc} are, respectively, the experimental melting enthalpy and the cold crystallization enthalpy obtained for the samples, ΔH_m^0 is the melting enthalpy of the 100%

PLA (93.0 J/g (Fukushima et al., 2011)) and wt.% clay is the weight percentage of the incorporated clay.

Results and discussion

Micrographs of the fractured surface of PLA nanocomposites with 3 and 5wt. % of clay minerals incorporation are shown in Fig. 1. A good dispersion degree of clay particles without aggregates in the micron range can be observed in the micrographs of the samples containing 3wt. % of C30B and D43B. Contrarily, the sample with 5wt. % of D43B exhibits some clay aggregates dispersed in the polymeric matrix. The incorporation of 3 and 5wt. % of C15A results in worse level of clay minerals dispersion since more clay aggregates were observed.

The better dispersion achieved with C30B can be associated to the strong interactions between the carbonyl functions of PLA chains and hydroxyl functions of C30B, which seem to improve the dispersion of this clay mineral in the PLA matrix (Fukushima et al., 2011; Solarski et al., 2007).

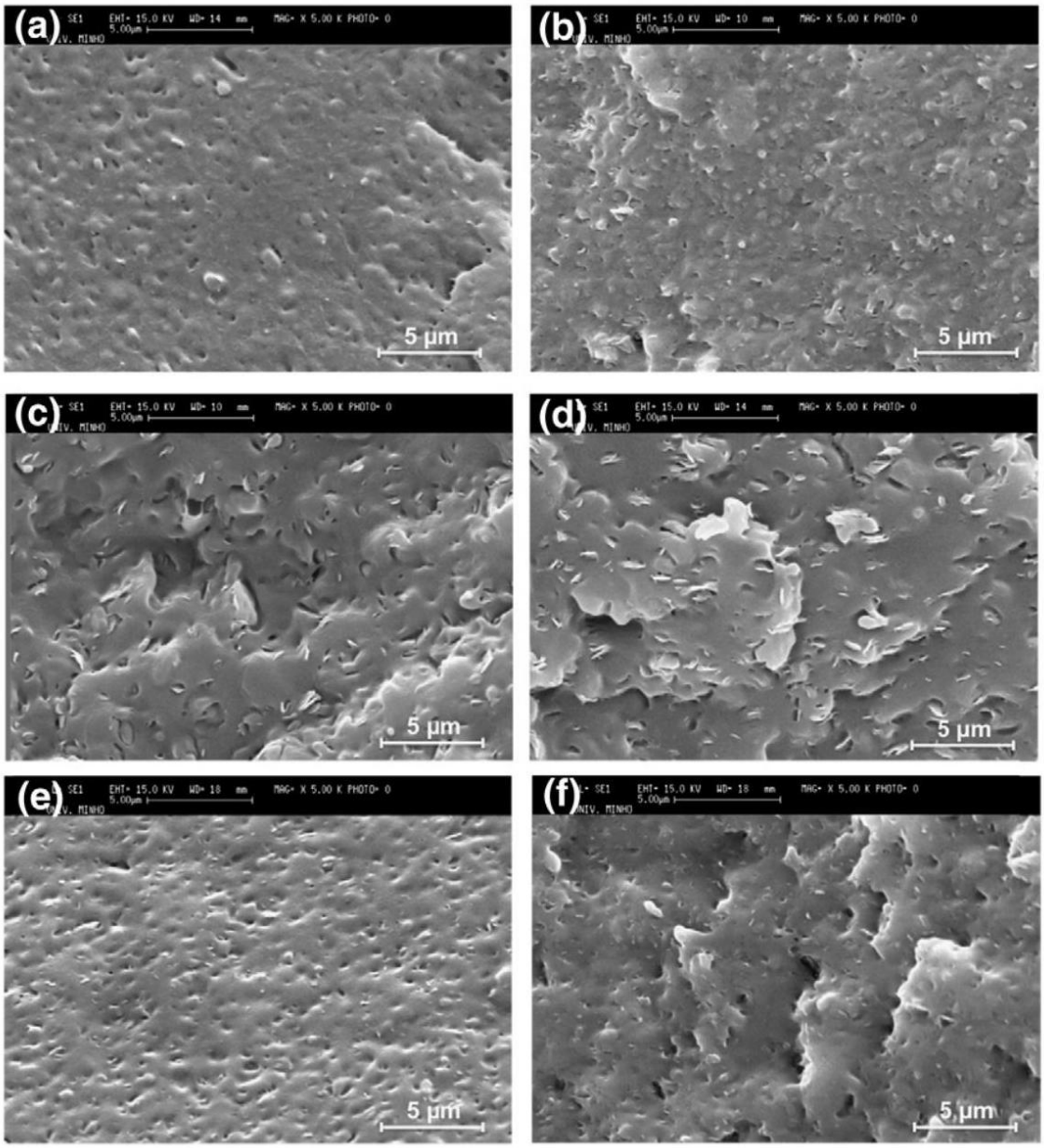

Fig. 1. SEM micrographs of (a) PLA with 3 wt. % C30B, (b) PLA with 5 wt. % C30B, (c) PLA with 3 wt. % C15A, (d) PLA with 5 wt. % C15A, (e) PLA with 3 wt. % D43B and (f) PLA with 5 wt. % D43B.

Since the SEM results showed that, in all cases with 5wt. % of clay minerals it was not possible to achieve good dispersion, only the nanocomposites prepared with 3wt. % were investigated.

XRD was also used to evaluate the nanocomposite structure, since the position, shape, and intensity of the different peaks may allow to evaluate the dispersion of mineral sheets within the polymer matrix (Sinha Ray and Okamoto, 2003; Zaidi et al., 2010). Fig. 2 shows, as an example, the X-ray patterns of the clay mineral C30B and the correspondent nanocomposites. The d-spacing values (basal distance between clay layers) were

calculated using Bragg's law ($\lambda = 2\,\mathrm{d}\sin\theta$; d is the interlayer d -spacing and λ is the wavelength) and results are presented in Table 2. The calculated d_{001} distance expands 1.60 for PLA/C30B, 0.62 for PLA/C15A and 1.65 nm for PLA/D43B. According to these results, PLA macromolecules diffused and were inserted between the clay mineral layers and nanocomposites with an intercalated structure were obtained. While the nanocomposites prepared with C30B and D43B present higher increase of interlayer separation, the one with C15A shows less. These results are in agreement with SEM results, which indicate that clay aggregates were formed in PLA/C15A nanocomposites. ^{1}H NMR analyses were performed for PLA and PLA nanocomposites containing C30B non-exposed and after 120 h of thermo-oxidative degradation. The chemical shift (δ) values obtained in the ^{1}H NMR spectra, the corresponding groups and integration values are listed in Table 3. It can be perceived that the assignments obtained are in well agreement with literature (Liu et al., 2006). No changes in chemical shift values are observed among all samples. However, differences in the signal intensities can be noticed. The proton intensity ratio (CH_3/CH) has a theoretical value of 3 and this ratio must remain constant if degradation takes place upon ester linkage degradation, hydrolysis or radical degradation, among others (Carrasco et al., 2010). The proton intensity ratio for PLA 0 h is 3.71 and for PLA 120 h is 2.97 , for C30B 0 h is 3.22 and for C30B 120 h is 3.07 . According to the literature (Carrasco et al., 2010) only pyrolytic elimination (which is responsible for the transformation of $CH-CH_3$ into $CH=CH_2$) can be responsible for a lower ratio. But this mechanism, if present, must be a secondary and less important degradation pathway since there was no signal for CH_2 protons in ^{1}H NMR. Comparing PLA and C30B samples, the decrease of proton intensity ratio is higher for PLA, which can be related with different extent of thermal degradation.

GPC results of PLA and nanocomposites before and after 120 h of thermo-oxidative degradation are depicted in Fig. 3. The results of the non degraded samples showed very slight degradation of PLA matrix during nanocomposite preparation, which can be attributed to hydrolysis reaction under the processing conditions used. After 120 h of thermal degradation, all samples exhibit a significant decrease in molecular weight together with a narrower and a shift of the molecular

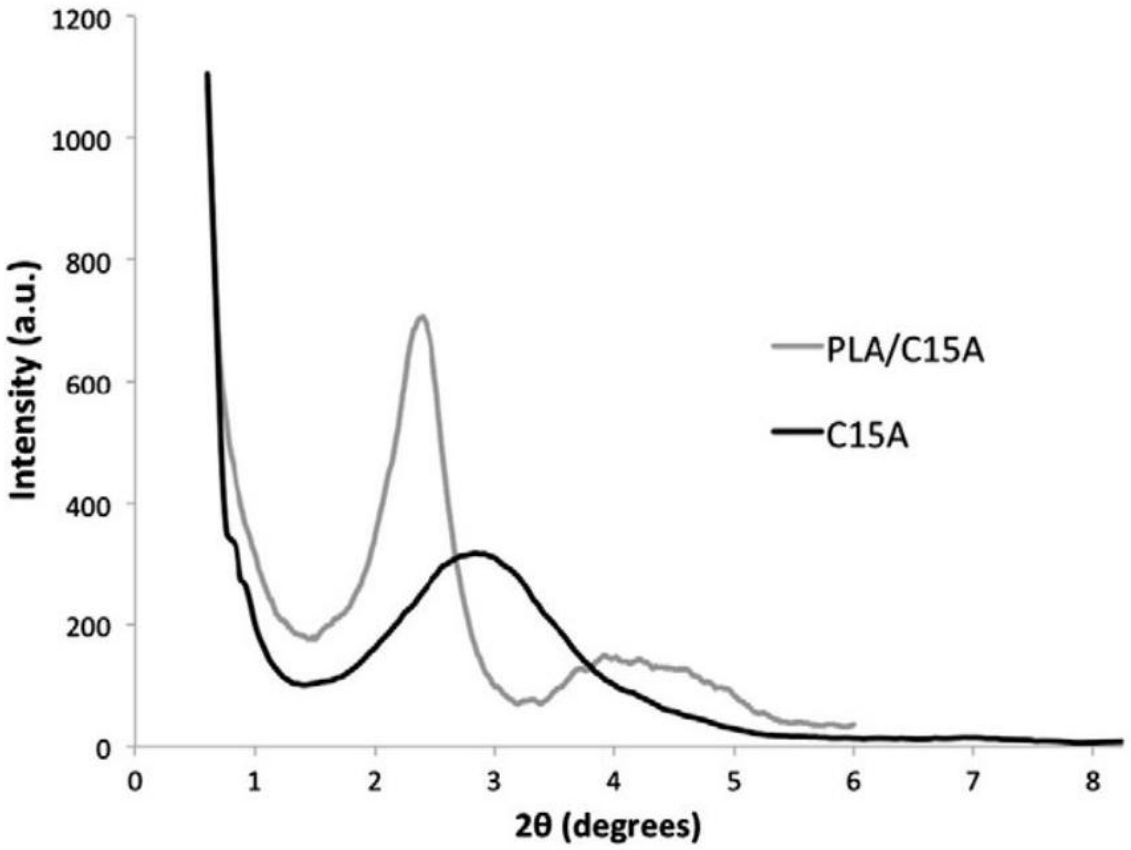

Fig. 2. X-ray diffractogram recorded for C15A and respective nanocomposites.

Table 2
d-Spacing values for clays and respective nanocomposites.

	d_{001}(nm)		
	C30B	C15A	D43B
Clay	2.07	3.07	1.87
Nanocomposite	3.67	3.69	3.52

weight distribution to lower molecular weight. This can be associated to the hydrolysis reaction leading to chain scission of the high molecular weight PLA molecules that resulted in smaller and more similar molecules. Moreover, taking into account the error associated with these measurements, the decrease of molecular weight is similar for all nanocomposites and slightly higher than for PLA. Since the molecular weight difference between initial and degraded nanocomposites with D43B was lower, it seems that the addition of D43B enhances the PLA thermal stability. An explanation for the different behaviors among the clay minerals, resides in their chemical composition and structure. Mts, belong to the family of 2:1 layered silicates, where negative charged platelets are counterbalanced by alkali and alkali earth cations (Na^+, Ca^{2+}, etc.) located in the galleries, which increases the clay hydrophilic character (Bordes et al., 2009). C30B modifier (MT_2EtOH, Table 1) introduced OH groups, which increase its hydrophilicity that is

associated to the good clay dispersion achieved (Fig. 1), enhance the hydrolysis of PLA macromolecule (Solarski et al., 2008) results in a higher chain scission when compared to D43B. On the other hand, D43B, due to the benzene ring, is more hydrophobic than C15A and C30B (MINERARIA, 2013). This property improves the dispersion of D43B in the PLA, since PLA is a hydrophobic polymer due to the presence of $-CH_3$ side groups (Vroman and Tighzert, 2009). Moreover, the capability of D43B to absorb moisture is lower, comparatively to C15A and C30B, acting as barrier retarding the degradation process (Vroman and Tighzert, 2009).

FTIR spectra of PLA and PLA nanocomposites with 3wt.% of C30B obtained before and after 24, 96 and 120 h of thermo-oxidative degradation are presented in Figs. 4 and 5. The addition of clay minerals cannot be detected in initial FTIR spectra of nanocomposites when compared to PLA. This fact can indicate that the clay minerals didn't change the degradation mechanism of PLA. In Fig. 4a an increase of the bands in the 3600-3500 cm^{-1} region, assigned to OH end groups (Matusik et al., 2011; Wu et al., 2009) and free hydroxyl groups (Zaidi et al., 2010), can be observed along degradation time, as well as, a decrease in the bands $3000 - 2800$ cm^{-1} attributed to CH deformation (including symmetric and asymmetric bends) (Kister et al., 1998; Liu et al., 2006; Zaidi et al., 2010). A large and saturated band around 1750 cm^{-1}, assigned to C=O from ester groups (Liu et al., 2006; Zaidi et al., 2010), in Fig. 4b, shows two new shoulders at 1724 and 1714 cm^{-1}, after degradation associated to the formation of new carbonyl compounds. A huge reduction in the band around $1380 - 1310$ cm^{-1} attributed to CH linkages (Kister et al., 1998; Liu et al., 2006; Zaidi et al., 2010) (Fig. 4c) can be detected after degradation, which is in agreement with what was observed in Fig. 4a. Crystallization leads to a decrease of the band at 1267 cm^{-1} (Meaurio et al., 2006) assigned to CO stretch (Kister et al., 1998; Liu et al., 2006; Zaidi et al., 2010). In the region from 1000 to 500 cm^{-1}, shown in Fig. 4d, a decrease of the amorphous band at 955 cm^{-1}

Table 3
^{1}H NMR data for PLA samples.

	δCH_3 (ppm)	Integration	δCH (ppm)	Integration	Proton intensity ratio (CH_3/CH)
Literature (Liu et al., 2006)	1.51-1.56	-	5.11-5.24	-	-
PLA 0 h	1.56-1.60	78.76	5.14-5.21	21.24	3.71
PLA 120 h	1.58-1.60	74.81	5.13-5.21	25.19	2.97
C30B 0 h	1.571	76.29	5.16	23.71	3.22
C30B 120 h	1.57	75.43	5.15	24.57	3.07

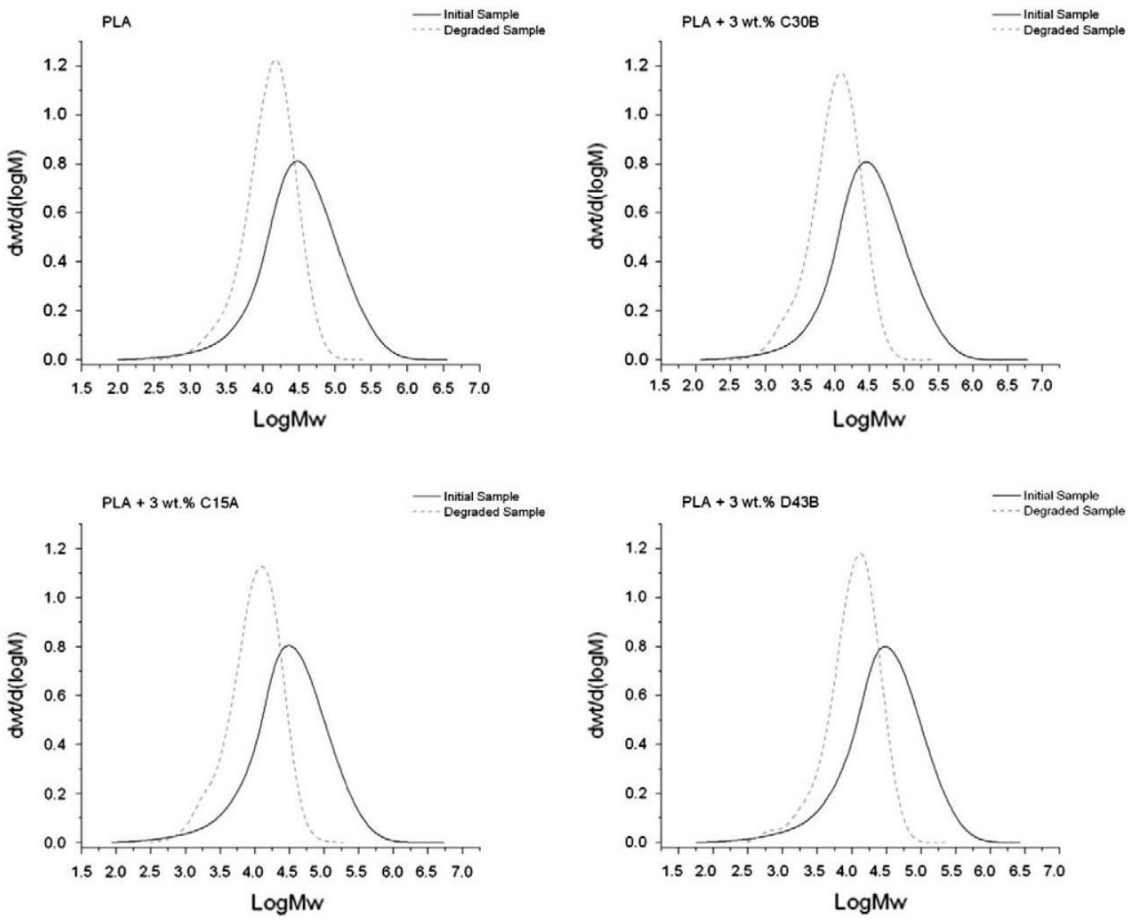

Fig. 3. Molecular weight distribution of initial and degraded samples.

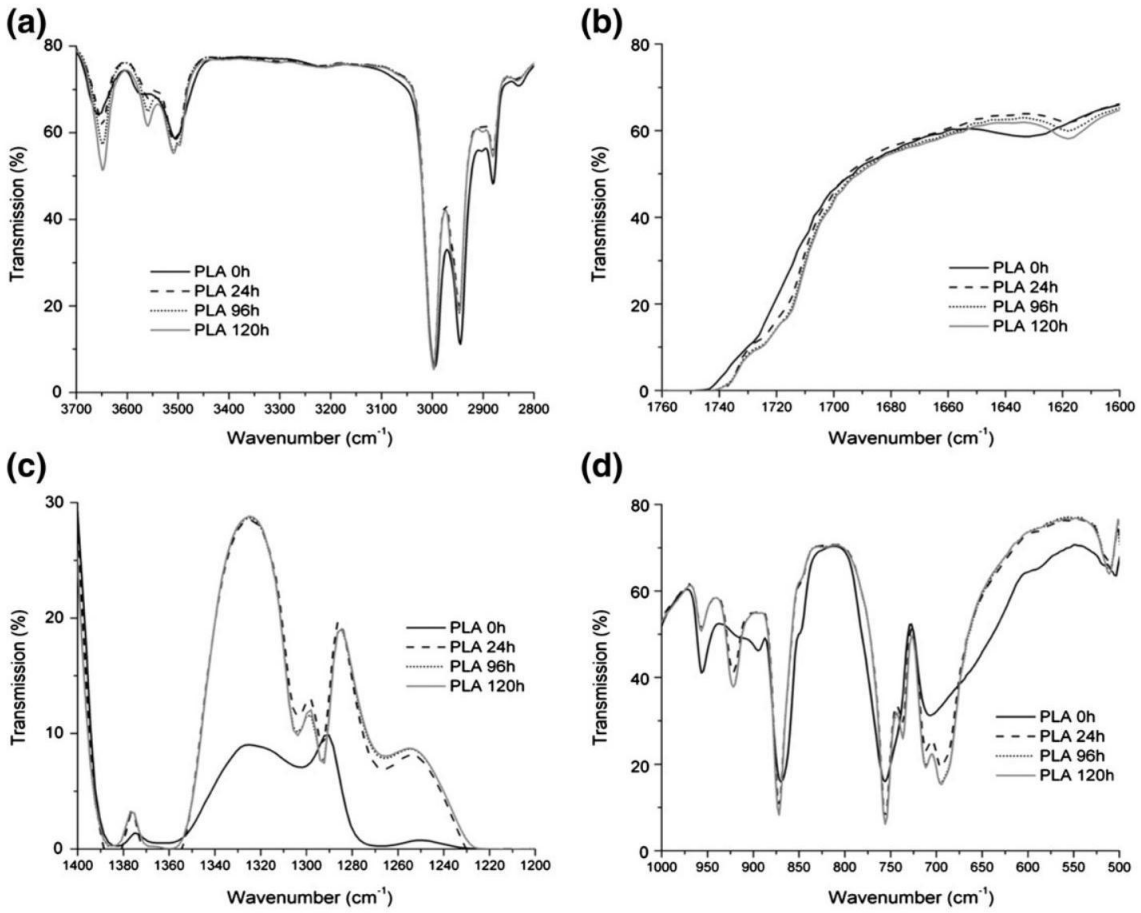

Fig. 4. FTIR spectra of PLA obtained before and after 24,96 and 120 h of thermo-oxidative degradation.

(Meaurio et al., 2006) assigned to CH_3 and CC linkages (Kister et al., 1998; Liu et al., 2006) can be observed together with the appearance of a new band at 920 cm^{-1}, characteristic of α crystals. It is known that the band at 869 cm^{-1} is assigned to the amorphous phase and the band at 755 cm^{-1} to the crystalline phase (Liu et al., 2006; Wu et al., 2009), and along degradation a small increase of both bands, C-COO and C-O vibrations, were observed (Kister et al., 1998; Liu et al., 2006; Wu et al., 2009; Zaidi et al., 2010). An increase and unfolding of the band around 700 cm^{-1}, which corresponds to $C = 0$ (Kister et al., 1998) were also detected.

FTIR spectra obtained for PLA with 3 wt.% C30B are depicted in Fig. 5. The overall FTIR spectrum is quite similar to the one obtained for PLA (Fig. 4), no vibration modes are totally suppressed and no new modes seem to appear due to the clay presence. PLA structure changes due to degradation but not with clay addition. The results obtained with different clay minerals were similar (results not shown).

Thermal properties of PLA and PLA nanocomposites were evaluated by DSC. Fig. 6 presents the crystallinity degree of PLA and PLA nanocomposites with 3wt. % clay before and after 120 h of thermal degradation. It is known that the addition of the clay minerals promotes the extent of crystallization of PLA during heating indicating that they can act as nucleating agents (Fukushima et al., 2011; Lewitus et al., 2006). This was observed for C30B and D43B probably due to the good dispersion achieved (Fig. 1). With the

incorporation of C15A a non-expected decrease in crystallinity degree was observed, probably due to the heterogeneity and aggregate formation observed in this sample. After 120 h of thermal degradation, although an increase of the crystallinity degree can be detected for all samples, it was higher for nanocomposites. This increase is due to the hydrolysis of the PLA chains, in the

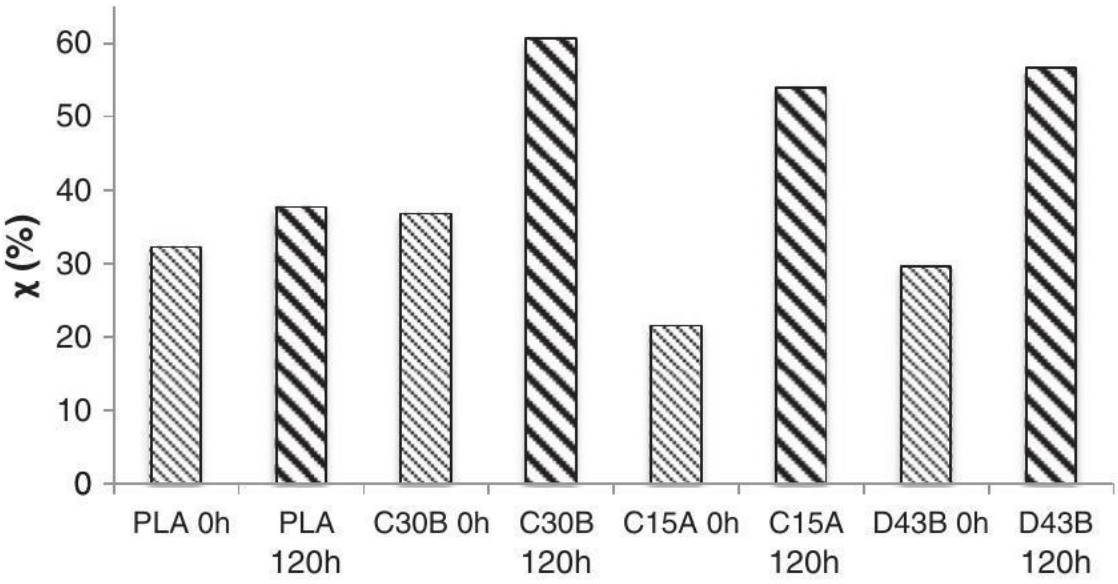

Fig. 6. Crystallinity degree (χ) of initial and degraded samples with 3wt% clay incorporation.

amorphous region rather than in the crystalline region because they are more accessible. The shorter PLA chains, as shown by GPC (Fig. 5), have higher mobility and they can reorganize easily, which leads to an increase of crystallinity degree (Solarski et al., 2008; Zaidi et al., 2010). As expected, due to the higher chain scission induced by hydroxyl groups, the nanocomposite with C30B presents higher crystallinity degree after degradation.

Table 4 presents T_g and T_m values obtained from DSC analysis. It can be firstly noted that the PLA T_g in the nanocomposites appears to be slightly higher than PLA. This behavior has been observed by other authors (Sinha Ray et al., 2003; Zhou and Xanthos, 2009) and ascribed to the restricted segmental motions at the organic-inorganic interface neighborhood of intercalated compositions. Regarding to T_m of PLA

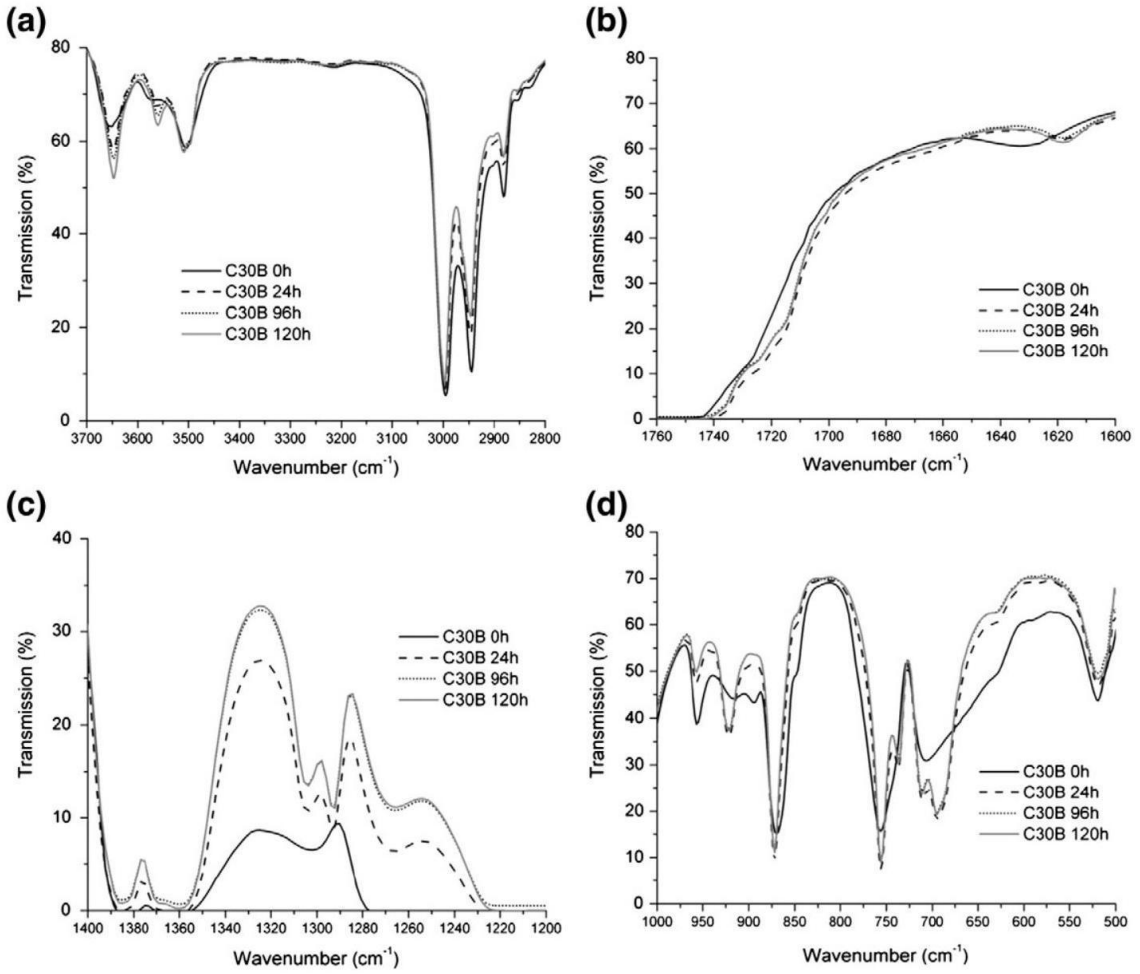

Fig. 5. FTIR spectra of PLA with 3wt. %C30 B obtained before and after 24,96 and 120 h of thermo-oxidative degradation.

Table 4
T_m and T_g results obtained for PLA and PLA nanocomposites with 3wt. % clay incorporation.

Samples	T_g (°C)	T_m (°C)
PLA 0 h	48.5	164.5
PLA 120 h	-	164.5
PLA C30B 0 h	57.3	166.6
PLA C30B 120 h	-	164.8
PLA C15A 0 h	50.7	164.9
PLA C15A 120 h	-	164.6
PLA D43B 0 h	50.3	164.5

PLA D43B 120 h	-	164.7

and nanocomposites, the incorporation of clays does not affect it, similar temperatures were obtained, which are in agreement with other authors (Kubies et al., 2006; Paul et al., 2003).

Conclusion

In this work, the effect of different organically modified Mts (Cloisite 30B, Cloisite 15A and Dellite 43B) and their amounts (3 and 5% in weight) on the thermo-oxidative aging of PLA was investigated. According to SEM and XRD results, better clay mineral dispersion was achieved with 3wt. % for PLA nanocomposites prepared with C30B and D43B. Results from ^{1}H NMR and GPC demonstrated that chain scission occurs after 120 h of degradation. The addition of D43B seemed to contribute to higher thermal stability of PLA nanocomposites since the molecular weight difference between initial and degraded samples was smaller.

DSC results evidence an increase of the crystallinity degree of the samples after addition of the nanoclays and after degradation.

Acknowledgments

This work was funded by PEst-C/QUI/UI0686/2011 and PEst-C/CTM/ LA0025/2011. Thanks are due to the National NMR Network that was purchased within the framework of the National Program for Scientific Re-equipment, contract REDE/1517/RMN/2005 with funds from POCI 2010 (FEDER) and FCT.

References

Badía, J.D., Strömberg, E., Ribes-Greus, A., Karlsson, S., 2011. Assessing the MALDI-TOF MS sample preparation procedure to analyze the influence of thermo-oxidative ageing and thermo-mechanical degradation on poly(lactide). Eur. Polym. J. 47 (7), 1416-1428.
Bikiaris, D., 2011. Can nanoparticles really enhance thermal stability of polymers? Part II: an overview on thermal decomposition of polycondensation polymers. Thermochim. Acta 523 (1-2), 25-45.
Bordes, P., Pollet, E., Averous, L., 2009. Nano-biocomposites: biodegradable polyester/ nanoclay systems. Prog. Polym. Sci. 34 (2), 125-155.
Carrasco, F., Pagès, P., Gámez-Pérez, J., Santana, O.O., Maspoch, M.L., 2010. Processing of poly(lactic acid): characterization of chemical structure, thermal stability and mechanical properties. Polym. Degrad. Stab. 95 (2), 116-125.
Carrasco, F., Gámez-Pérez, J., Santana, O.O., Maspoch, M.L., 2011. Processing of poly(lactic acid)/organomontmorillonite nanocomposites: microstructure, thermal stability and kinetics of the thermal decomposition. Chem. Eng. J. 178, 451-460.
Chang, J.H., An, Y.U., Cho, D., Giannelis, E.P., 2003a. Poly(lactic acid) nanocomposites: comparison of their properties with montmorillonite and synthetic mica (II). Polymer 44 (13), 3715-3720.
Chang, J.H., An, Y.U., Sur, G.S., 2003b. Poly (lactic acid) nanocomposites with various

organoclays. I. Thermomechanical properties, morphology, and gas permeability. J. Polym. Sci. B Polym. Phys. 41 (1), 94-103.

Chow, W., Lok, S., 2009. Thermal properties of poly(lactic acid)/organo-montmorillonite nanocomposites. J. Therm. Anal. Calorim. 95 (2), 627-632.

Fukushima, K., Abbate, C., Tabuani, D., Gennari, M., Camino, G., 2009. Biodegradation of poly(lactic acid) and its nanocomposites. Polym. Degrad. Stab. 94 (10), 1646-1655.
Fukushima, K., Tabuani, D., Dottori, M., Armentano, I., Kenny, J.M., Camino, G., 2011. Effect of temperature and nanoparticle type on hydrolytic degradation of poly(lactic acid) nanocomposites. Polym. Degrad. Stab. 96 (12), 2120-2129.
Gardette, M., Thérias, S., Gardette, J.-L., Murariu, M., Dubois, P., 2011. Photooxidation of polylactide/calcium sulphate composites. Polym. Degrad. Stab. 96 (4), 616-623.
Kister, G., Cassanas, G., Vert, M., 1998. Effects of morphology, conformation and configuration on the IR and Raman spectra of various poly(lactic acid)s. Polymer 39 (2), 267-273.
Kubies, D., Ščudla, J., Puffr, R., Sikora, A., Baldrian, J., Kovářová, J., Šlouf, M., Rypáček, F., 2006. Structure and mechanical properties of poly(L-lactide)/layered silicate nanocomposites. Eur. Polym. J. 42 (4), 888-899.
Lewitus, D., McCarthy, S., Ophir, A., Kenig, S., 2006. The effect of nanoclays on the properties of PLLA-modified polymers part 1: mechanical and thermal properties. J. Polym. Environ. 14 (2), 171-177.
Liu, X., Zou, Y., Li, W., Cao, G., Chen, W., 2006. Kinetics of thermo-oxidative and thermal degradation of poly(D,L-lactide) (PDLA) at processing temperature. Polym. Degrad. Stab. 91 (12), 3259-3265.
Madhavan Nampoothiri, K., Nair, N.R., John, R.P., 2010. An overview of the recent developments in polylactide (PLA) research. Bioresour. Technol. 101 (22), 8493-8501.
Matusik, J., Stodolak, E., Bahranowski, K., 2011. Synthesis of polylactide/clay composites using structurally different kaolinites and kaolinite nanotubes. Appl. Clay Sci. 51 (1-2), 102-109.
Meaurio, E., Lopez-Rodriguez, N., Sarasua, J., 2006. Infrared spectrum of poly(l-lactide): application to crystallinity studies. Macromolecules 39 (26), 9291-9301.
MINERARIA, L.C., 2013. Dellite 43B [Online]. [Accessed 13-11-2013].
Mülhaupt, R., 2013. Green polymer chemistry and bio-based plastics: dreams and reality. Macromol. Chem. Phys. 214 (2), 159-174.
Nieddu, E., Mazzucco, L., Gentile, P., Benko, T., Balbo, V., Mandrile, R., Ciardelli, G., 2009. Preparation and biodegradation of clay composites of PLA. React. Funct. Polym. 69 (6), 371-379.

Nishida, H., Mori, T., Hoshihara, S., Fan, Y., Shirai, Y., Endo, T., 2003. Effect of tin on poly(Llactic acid) pyrolysis. Polym. Degrad. Stab. 81 (3), 515-523.
Paul, M.A., Alexandre, M., Degée, P., Henrist, C., Rulmont, A., Dubois, P., 2003. New nanocomposite materials based on plasticized poly(L-lactide) and organo-modified montmorillonites: thermal and morphological study. Polymer 44 (2), 443-450.
Paul, M.A., Delcourt, C., Alexandre, M., Degée, P., Monteverde, F., Dubois, P., 2005. Polylactide/montmorillonite nanocomposites: study of the hydrolytic degradation. Polym. Degrad. Stab. 87 (3), 535-542.
Picard, E., Espuche, E., Fulchiron, R., 2011. Effect of an organo-modified montmorillonite on PLA crystallization and gas barrier properties. Appl. Clay Sci. 53 (1), 58-65.
Pluta, M., Galeski, A., Alexandre, M., Paul, M.A., Dubois, P., 2002. Polylactide/montmorillonite nanocomposites and microcomposites prepared by melt blending: structure and some physical properties. J. Appl. Polym. Sci. 86 (6), 1497-1506.

Rhim, J.-W., Hong, S.-I., Ha, C.-S., 2009. Tensile, water vapor barrier and antimicrobial properties of PLA/nanoclay composite films. LWT Food Sci. Technol. 42 (2), 612-617.
Sinha Ray, S., Okamoto, M., 2003. Polymer/layered silicate nanocomposites: a review from preparation to processing. Prog. Polym. Sci. 28 (11), 1539-1641.
Sinha Ray, S., Yamada, K., Okamoto, M., Fujimoto, Y., Ogami, A., Ueda, K., 2003. New polylactide/layered silicate nanocomposites. 5. Designing of materials with desired properties. Polymer 44 (21), 6633-6646.
Sinharay, S., Bousmina, M., 2005. Biodegradable polymers and their layered silicate nanocomposites: in greening the 21st century materials world. Prog. Mater. Sci. 50 (8), 962-1079.
Solarski, S., Mahjoubi, F., Ferreira, M., Devaux, E., Bachelet, P., Bourbigot, S., Delobel, R., Coszach, P., Murariu, M., Da silva Ferreira, A., 2007. (Plasticized) Polylactide/clay nanocomposite textile: thermal, mechanical, shrinkage and fire properties. J. Mater. Sci. 42 (13), 5105-5117.
Solarski, S., Ferreira, M., Devaux, E., 2008. Ageing of polylactide and polylactide nanocomposite filaments. Polym. Degrad. Stab. 93 (3), 707-713.
Vroman, I., Tighzert, L., 2009. Biodegradable polymers. Materials 2 (2), 307-344.
Wu, T.-M., Wu, C.-Y., 2006. Biodegradable poly(lactic acid)/chitosan-modified montmorillonite nanocomposites: preparation and characterization. Polym. Degrad. Stab. 91 (9), 2198-2204.

Wu, X., Yuan, J., Yu, Y., Wang, Y., 2009. Preparation and characterization of polylactide/montmorillonite nanocomposites. J. Wuhan Univ. Technol.-Mater. Sci. Ed. 24 (4), 562-565.
Zaidi, L., Kaci, M., Bruzaud, S., Bourmaud, A., Grohens, Y., 2010. Effect of natural weather on the structure and properties of polylactide/Cloisite 30B nanocomposites. Polym. Degrad. Stab. 95 (9), 1751-1758.
Zhou, Q., Xanthos, M., 2009. Nanosize and microsize clay effects on the kinetics of the thermal degradation of polylactides. Polym. Degrad. Stab. 94 (3), 327-338.
Zhu, H., Zhu, Q., Li, J., Tao, K., Xue, L., Yan, Q., 2011. Synergistic effect between expandable graphite and ammonium polyphosphate on flame retarded polylactide. Polym. Degrad. Stab. 96 (2), 183-189.

---

[a] T is tallow (~ 65% C18; ~ 30% C16; ~ 5% C14).